Eur. Phys. J. C 18, 317–325 (2000)
Digital Object Identifier (DOI) 10.1007/s100520000543

THE EUROPEAN
PHYSICAL JOURNAL C
© Società Italiana di Fisica
Springer-Verlag 2000

Space-time evolution of the hadronic source in peripheral to central Pb+Pb collisions

I.G. Bearden[1], H. Bøggild[1], J. Boissevain[2], P.H.L. Christiansen[1], L. Conin[4], J. Dodd[3], B. Erazmus[4], S. Esumi[5,a], C.W. Fabjan[6], D. Ferenc[7,b], A. Franz[6,c], J.J. Gaardhøje[1], A.G. Hansen[1,d], O. Hansen[1], D. Hardtke[9,e], H. van Hecke[2], E.B. Holzer[6], T.J. Humanic[9], P. Hummel[6], B.V. Jacak[10], K. Kaimi[5,f], M. Kaneta[5,e], T. Kohama[5], M. Kopytine[10,g], M. Leltchouk[3], A. Ljubičić Jr.[7,c], B. Lörstad[11], N. Maeda[5,h], L. Martin[4], A. Medvedev[3], M. Murray[8], H. Ohnishi[5,c], G. Paić[6,9], S.U. Pandey[9,i], F. Piuz[6], J. Pluta[4,j], V. Polychronakos[12], M. Potekhin[3], G. Poulard[6], D. Reichhold[9,k], A. Sakaguchi[5,l], J. Schmidt-Sørensen[11], J. Simon-Gillo[2,m], W. Sondheim[2], T. Sugitate[5], J.P. Sullivan[2], Y. Sumi[5,n], W.J. Willis[3], K. Wolf[8,f], N. Xu[2,e], D.S. Zachary[9]

[1] Niels Bohr Institute, 2100 Copenhagen, Denmark
[2] Los Alamos National Laboratory, Los Alamos, NM 87545, USA
[3] Department of Physics, Columbia University, New York, NY 10027,USA
[4] Nuclear Physics Laboratory of Nantes, 44072 Nantes, France
[5] Hiroshima University, Higashi-Hiroshima 739-8526, Japan
[6] CERN, 1211 Geneva 23, Switzerland
[7] Rudjer Bošković Institute, Zagreb, Croatia
[8] Cyclotron Institute, Texas A&M University, College Station, TX 77843, USA
[9] Department of Physics, The Ohio State University, Columbus, OH 43210, USA
[10] State University of New York, Stony Brook, NY 11973, USA
[11] Department of Physics, University of Lund, 22362 Lund, Sweden
[12] Brookhaven National Laboratory, Upton, NY 11973, USA

Received: 17 July 2000 / Revised version: 3 November 2000 /
Published online: 8 December 2000 – © Springer-Verlag 2000

Abstract. Two-particle correlations of negative pions as a function of charged particle multiplicity are studied in Pb+Pb collisions at $\sqrt{s} = 17.3$GeV per nucleon using the NA44 experiment at the CERN Super Proton Synchrotron(SPS). We find that the source size parameters increase with the charged particle multiplicity. However the slope of the source size parameters plotted as a function of charged multiplicity is slightly larger at high multiplicity than at low multiplicity. The value of λ is independent of charged multiplicity. For Pb+Pb collisions, R_L is larger than R_{TS} and R_{TO} for all multiplicity intervals, whereas these three radius parameters were approximately equal in S+Nucleus collisions. The ratios (R_L/R_{TS}) and (R_L/R_{TO}) for Pb+Pb data show almost no dependence on charged multiplicity. The duration of pion emission $\Delta\tau$ is constant at 3.8±1.1 fm/c as a function of the charged multiplicity in Pb+Pb collisions. Effective volume (V) is also calculated as V=$\pi \times R_{TS}^2 \times R_L$, assuming a cylindrically shaped source. We found, within the limited statistics, the effective volume rapidly increases at high multiplicity.

1 Introduction

Heavy ion collisions at relativistic energies offer a possibility of producing highly condensed nuclear matter which may undergo a phase transition to a deconfined state,

[a] *now at* Heidelberg University, 69120 Heidelberg, Germany.
[b] *now at* University of California, Davis, CA 95616, USA
[c] *now at* Brookhaven National Laboratory, Upton, NY 11973, USA.
[d] *now at* Los Alamos National Laboratory, Los Alamos, NM 87545, USA.
[e] *now at* Lawrence Berkeley National Laboratory, Berkeley,CA 94720, USA
[f] *d*eceased
[g] *o*n an unpaid leave from P.N.Lebedev Physical Institute, Russian Academy of Sciences.
[h] *now at* Florida State University, Tallahassee, FL 32306, USA.
[i] *now at* Wayne State University, Detroit, MI 48202, USA.
[j] *now at* Institute of Physics, Warsaw University of Technology, Koszykowa 75,00-662, Warsaw, Poland.
[k] *now at* Creighton University, Omaha, NE 68178, USA.
[l] *now at* Osaka University, Toyonaka, Osaka 560-0043, Japan.
[m] *now at* U.S. Department of Energy, Germantown, MD 20874-1290, USA.
[n] *now at* Hiroshima International University, 555-36 Kurosecho, Hiroshima 724-0695, Japan

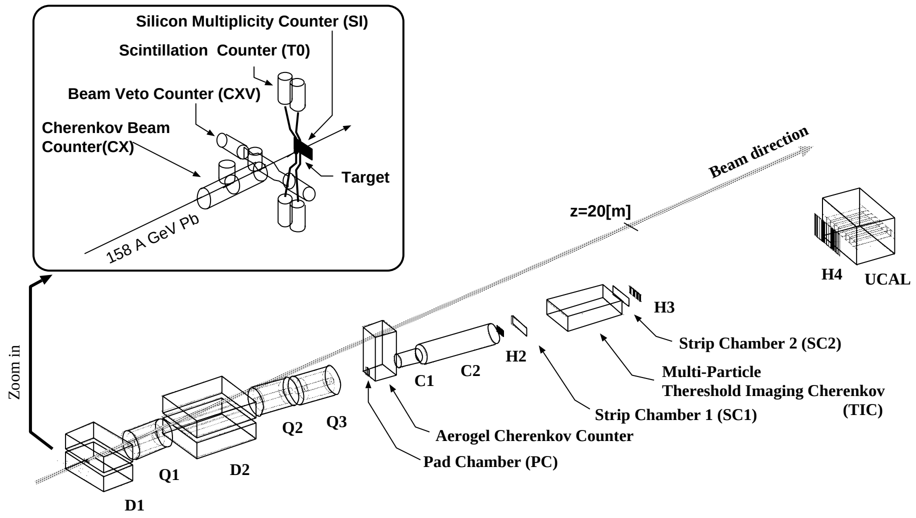

Fig. 1. The NA44 experimental setup for Pb+Pb running

the Quark Gluon Plasma(QGP). For central Pb+Pb collisions at $\sqrt{s} = 17.3$GeV per nucleon the energy density based on calorimetric measurements is estimated to reach 3 GeV/fm^3 [1]. According to lattice calculations this energy density should be sufficient to generate the QGP and indeed a dramatic suppression of the J/ψ yield and an enhancement of multi-strange baryons have been reported [2–4]. Both these effects are consistent with the existence of a plasma [5,6].

However such a phase transition should also make a significant difference in the Equation of State of nuclear matter and may therefore reveal itself in the space-time evolution of the source. Long particle emission duration is an expected signal of a first-order phase transition [7]. Two-particle interferometry is sensitive to this evolution and can thus play a crucial role in searching for a phase transition. Multi-dimensional correlation function analysis allows extraction of the duration of particle emission. We have studied the space-time extent of the particle source at freeze-out as a function of the charged multiplicity in heavy ion collisions. Previously we have reported that the size parameters in S+Nucleus collisions increase smoothly as a power function of charged multiplicity per unit rapidity, i.e as R=C$\cdot$(dN/dy)^a, where a=0.2 [8]. By comparing the multiplicity dependence in Pb+Pb collisions, we investigate to what extent the higher initial energy density alter the freeze-out conditions.

This paper presents two-particle correlation measurements as a function of charged multiplicity in Pb+Pb collisions at $\sqrt{s} = 17.3$GeV per nucleon. In Sect. 2, we describe the experimental setup. Section 3 gives the experimental procedure for the data analysis and the results of this analysis are given in Sect. 4. Section 5 discusses the extracted source size parameters, and conclusions are given in Sect. 6.

2 Experimental setup

The NA44 experiment measures one- and two-particle distributions of identified particles ($\pi^{\pm}, K^{\pm}, p, \bar{p}$) near mid-rapidity in heavy-ion collisions [8–11]. The setup of the experiment is shown schematically in Fig. 1. The 158 $\cdot$GeV/c per nucleon lead ion beam from the CERN/SPS goes through a Cherenkov beam counter (CX) [12] that has an intrinsic timing resolution of 35 ps and provides the start for the time of flight measurement. CX also effectively rejects pile up events. A plastic scintillation veto counter (CXV) with a 5 mm diameter hole just behind CX eliminates events from beam halo and particles produced by interactions upstream of the target. A lead disk target of 1 cm diameter and 2.27 g/cm^2 thickness was placed at the entrance of the first dipole magnet. The target thickness corresponds to 4.2% of an interaction length for a lead projectile. A scintillation counter (T0), just behind the target, is used to select centrality at the trigger level. A highly segmented silicon pad detector (SI) installed behind T0 measures the charged particle multiplicity. SI consists of 16 radial segments with equal pseudo-rapidity (η) bins and 32 azimuthal sectors. The pseudo-rapidity coverage of SI is from 1.5 to 3.3.

Two dipole magnets (D1 and D2) and three superconducting quadrupole magnets(Q1,Q2 and Q3) analyze the momenta of the secondary particles and create a magnified image of the target in the spectrometer. The data were taken at two focusing settings of the quadrupoles. These settings are referred to as horizontal and vertical focus.

The acceptance for the spectrometer is determined by the nominal momentum setting and angle. For these data the momentum range covers a band of $\pm 20\%$ about the nominal setting of 4 GeV/c. The spectrometer angle is set to 44 mrad with respect to the incident beam axis. The rapidity and transverse momentum(p_T) acceptance for pions in the horizontal and vertical settings is shown in Fig. 2. The mean p_T and rapidity are 143 MeV/c and 3.7, respectively, for the horizontal setting, and 173 MeV/c and 3.5, respectively, for the vertical setting.

A set of multi-wire proportional chambers with pad (PC) and strip (SC1 and SC2) readout and highly segmented scintillator hodoscopes (H2, H3 and H4) are placed after the spectrometer magnets to reconstruct the

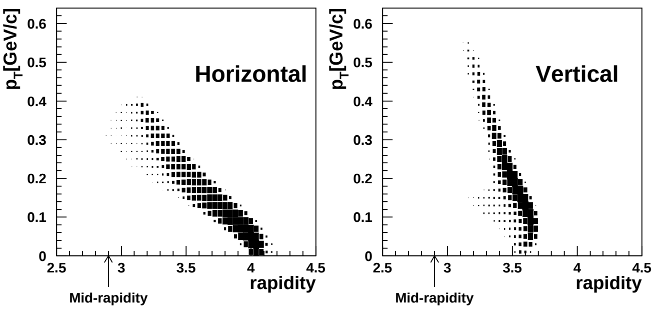

Fig. 2. The spectrometer acceptance for pions vs rapidity and p_T. The nominal momentum setting is 4GeV/c. The spectrometer angle is 44 mrad

tracks. The hodoscopes H2-4 are used to provide the stop signal for the Time of Flight(TOF) system. The details can be found elsewhere [13]. The overall TOF resolution is 95 ps with a flight length of 18m between CX and H3.

Three Cherenkov detectors, C1, C2 and a Threshold Imaging Cherenkov (TIC) detector [14–16], are also used for particle identification. For the momentum setting in this study, the velocities of electrons and pions are above the C1 threshold, while C2 is fired only by electrons. The signal from C2 is used as a Veto signal to eliminate events with electrons at the trigger level and the signal pulse height from C1 is used to improve the purity of pion pairs in our data sample in the off-line analysis. Pions with more than 2.5 GeV/c momentum produce Cherenkov light in the radiator of the TIC. The produced photons are detected track-by-track in a circular fiducial zone around the track. Ideally, kaon and proton tracks should have zero photons detected in this fiducial area. However, because of overlaps of fiducial areas of different tracks, the identification is achieved in practice by applying a threshold in the number of detected photons(hit pads) to identify a pion. The number of hit pads for each track is used to reject particles heavier than pions from the pion data samples.

The trigger signal($Trig$) for this study is made as follows;

$$Trig = CX \cap \overline{CXV} \cap T0 \cap \overline{C2} \cap PC \cap H2_{\geq 2} \cap H3_{\geq 2} \quad (1)$$

"$CX \cap \overline{CXV}$" is required to select "good beam" events. At least one hit on the PC and at least two hits on H2 and H3 are required to select 2 track events. The pulse height of T0 defines the centrality of the triggered events. The data used in this study are taken with two different centrality settings selected by T0 thresholds. One is "semi-central trigger", and the other is "central trigger". The trigger cross sections($\sigma_{Trig}/\sigma_{Total}$) are 28% and 9% for "semi-central trigger" and "central trigger" data, respectively.

3 Data analysis

Particle tracks are reconstructed using straight line fits to the hit positions on PC, H2, SC1, SC2 and H3. The momentum for each track is calculated from the hit positions on PC and H2, with resolution $\Delta p/p = 0.2\%$. The main

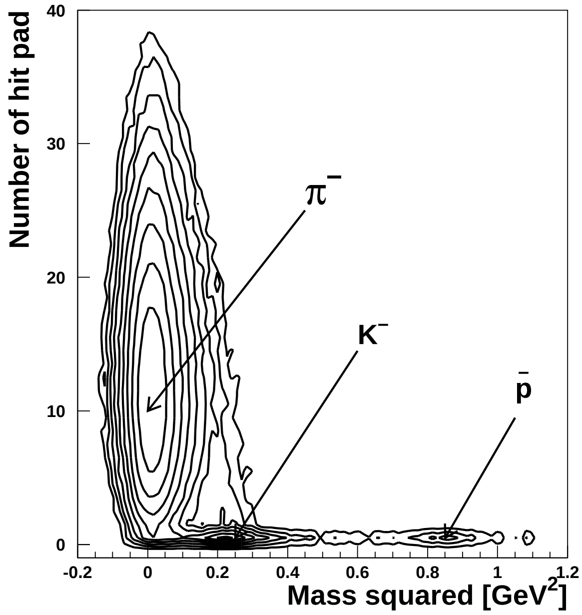

Fig. 3. The distribution of mass^2 vs number of hit pads in the TIC

Table 1. Trigger centrality and number of pion pairs for the data sets used in this analysis

Trigger	Centrality ($\sigma_{Trig}/\sigma_{Total}$)	Number of pairs Horizontal	Number of pairs Vertical
semi-central	28%	90 k	58 k
central	9%	343 k	276 k

uncertainty is from multiple scattering in the target and detector materials. Particle identification for each track uses the TOF at H3, the pulse height of C1 and the number of hit pads on the TIC around the reconstructed track. The events are selected by requiring a C1 pulse height corresponding to two or more pions. Figure 3 shows a plot of the mass squared distribution on H3 versus the number of hit pads in the TIC. A clear separation of the particle species is seen. The contamination of kaons and protons in our pion data sample is less than 1%. The total number of reconstructed pion pairs of "semi-central triggered" and "central triggered" data which used in this study are listed in Table 1.

The raw correlation function is calculated as follows:

$$C_{raw}(\mathbf{p_1}, \mathbf{p_2}) = \frac{Real(\mathbf{p_1}, \mathbf{p_2})}{Back(\mathbf{p_1}, \mathbf{p_2})}, \quad (2)$$

where $\mathbf{p_i}$ are the particle momenta. $Real(\mathbf{p_1}, \mathbf{p_2})$ is the distribution of relative momenta for "Real" pion pairs, and $Back(\mathbf{p_1}, \mathbf{p_2})$ is the "background distribution" created by mixing pairs from different events. Ten randomly selected background pairs are chosen for each real pair. Consequently, the number of the $Back(\mathbf{p_1}, \mathbf{p_2})$ pairs is 10 times higher than for $Real(\mathbf{p_1}, \mathbf{p_2})$, and the statistical error for the correlation function is dominated by $Real(\mathbf{p_1}, \mathbf{p_2})$. Pion pairs in $Back(\mathbf{p_1}, \mathbf{p_2})$ are subjected to the same

Table 2. The resolution of relative momenta Q_{TS}, Q_{TO} and Q_L in the LCMS frame

relative momentum resolution (MeV/c)					
horizontal			vertical		
Q_{TS}	Q_{TO}	Q_L	Q_{TS}	Q_{TO}	Q_L
7.9	13	7.9	18	19	8.2

analysis procedure and cuts as used for real pairs. The raw correlation function C_{raw} is distorted by the residual Bose-Einstein effect in the background distribution [17,18], the finite momentum resolution of the detector, the two-particle acceptance of the detectors and Coulomb repulsion between particles. Corrections for these effects must be applied to the raw correlation function. The true correlation function can be written as,

$$C_{corr}(\mathbf{p_1}\ ,\ \mathbf{p_2}) = C_{raw}(\mathbf{p_1},\mathbf{p_2}) \times K_{SPC}(\mathbf{p_1},\mathbf{p_2}) \\ \times K_{acceptance}(\mathbf{p_1},\mathbf{p_2}) \times K_{Coul}(\mathbf{p_1},\mathbf{p_2}), \quad (3)$$

where K_{SPC} is the correction for residual Bose-Einstein correlation in the background distribution, $K_{acceptance}$ corrects the distortion of the two-particle spectrum by the momentum resolution and two-particle acceptance [19] and K_{Coul} corrects for the effect of the repulsive Coulomb force between the particles in the pairs. In this study, the Coulomb wave integration method is used to generate K_{Coul} [20].

The fully corrected correlation function C_2 is fitted with the following three-dimensional Gaussian parameterization:

$$C_2 = 1 + \lambda\ exp(-R_{TS}^2 Q_{TS}^2 - R_{TO}^2 Q_{TO}^2 - R_L^2 Q_L^2). \quad (4)$$

The momentum difference $\mathbf{Q}(=\ \mathbf{p_1} - \mathbf{p_2})$ of the particle pair is resolved into two dimensions, perpendicular to the beam axis ($\mathbf{Q_T}$) and parallel to the beam axis (Q_L). $\mathbf{Q_T}$ is further separated into two dimensions: Q_{TO} is parallel to the sum of transverse momentum of particle pairs $\mathbf{k_T}$=$(\mathbf{p_{T1}} + \mathbf{p_{T2}})/2$, and Q_{TS} is perpendicular to $\mathbf{k_T}$. In this study, the Longitudinal Center of Mass System (LCMS) is chosen as reference frame ($p_{z1} + p_{z2} = 0$). The Q_{TS}, Q_{TO} and Q_L resolutions are listed in Table 2, and the acceptance in the horizontal and vertical settings is shown in Fig. 4. The data combined for both settings (horizontal and vertical) have enough acceptance in relative momentum space for a 3-dimensional analysis(Q_{TS}, Q_{TO} and Q_L). The correction factors ($K_{SPC}, K_{acceptance}$ and K_{Coul}) used to extract the "true" correlation depend on the source size parameters. Thus the correction of the raw correlation function is performed iteratively, fitting the correlation function with (4) [19].

The charged particle multiplicity was measured with SI. Beam particles create delta electrons in the target and air in front of the SI. The field in D1 sweeps these electrons to the left or right side of SI depending on whether the spectrometer is set for positive or negative particles. To eliminate the effect of the delta electrons, only one side of SI (the delta-clean side) was used to estimate the

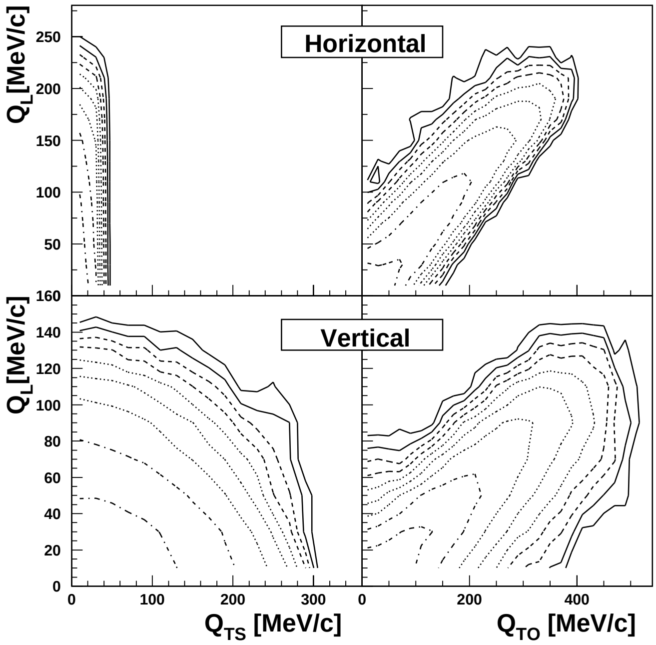

Fig. 4. The relative momentum acceptance for pions

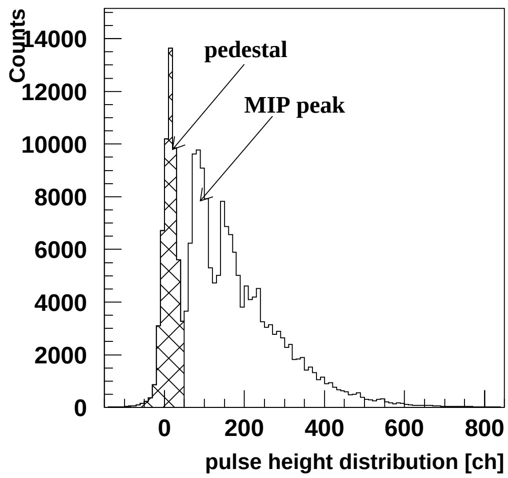

Fig. 5. Typical pulse height distribution for a silicon pad

multiplicity. As an example, the total number of charged particles in the part of the SI used in this analysis was 480 for the part with $\mathrm{d}N^{\pm}/\mathrm{d}\eta$=534. The occupancy was close to 100% at the highest multiplicity. The pulse height distributions were used to determine the total multiplicity [8]. As seen in Fig. 5, the pulse height distributions are able to distinguish one, two, and possibly three hit per pad. The multiplicity resolution at high multiplicity is around ± 7. The systematic error on the scale is 12%.

Systematic errors on the source size parameters were evaluated by changing parameters in the analysis procedure and refitting the correlation function. The parameters modified in this systematic error evaluation are as follows: (a) minimum two particle separation on the tracking detectors(PC, H2 and H3), (b) assumed momentum resolution changed by $\pm 20\%$, (c) the m_T slope parameter used to generate Monte-Carlo events was changed by 5%, (d)

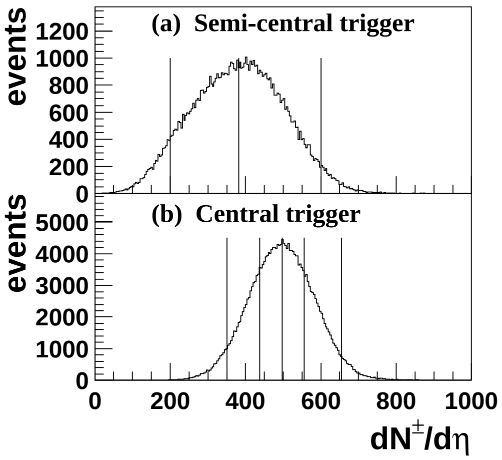

Fig. 6a,b. Multiplicity distribution $dN^{\pm}/d\eta$ for $1.5 < \eta < 3.3$ as measured SI. **a** is for semi-central events and **b** is for central triggered events. Multiplicity intervals are also shown by vertical lines

Table 3. Systematic errors on extracted source size parameters

source of systematic error	λ	R_{ts}	R_{to}	R_l
(a) 2-track separation	4%	5%	2%	2%
(b) Mom resolution	5%	4%	4%	5%
(c) MC slope parameter	5%	14%	5%	13%
(d) number of hits on strip chamber	14%	3%	6%	9%
Total	16%	16%	9%	17%

minimum number of Strip Chamber hits for a valid pair. The cuts on two-particle separation in the tracking detectors are used to eliminate the "ghost-tracks" created when a single hit in the pad-chamber is misinterpreted as two hits or a single particle hits two adjacent scintillator slats. The assumed momentum resolution in the Monte-Carlo is important in the correction of C_2 for the momentum resolution. Changing the m_T slope in the Monte-Carlo changes the distribution of Q values. The number of strip chamber hits should ideally be 8 (4 per track) for a good pair, but two tracks can hit the same strip. To improve efficiency, the reconstruction code accepts tracks with 3 or more strip chamber hits per track.

The uncertainties from these sources are summarized in Table 3. The total systematic errors from these sources are 16%, 16%, 9% and 17% for λ, R_{TS}, R_{TO} and R_L, respectively. Note that there are no expected systematic correlations between the measured multiplicities and the HBT source size parameters.

4 Results

The charged multiplicity distributions for "semi-central" and "central" triggered data are shown in Fig. 6. The "semi-central" triggered data were divided into 2 bins, while "central" triggered data were divided into 4 bins with an equal number of events in each multiplicity bin. The mean k_T of the pair is 164 MeV/c for all multiplicity intervals. The correlation functions for each multiplicity bin in the "central" triggered data are shown in Fig. 7, where the points are projections which extend over the lowest 30 MeV/c in the other directions of the momentum difference. The extracted source size parameters are listed in Table 4.

The source size parameters, λ, R_{TS}, R_{TO} and R_L, as a function of the charged multiplicity are shown in Fig. 8 and 9. The data points from S+Nucleus experiments [8] are also plotted on the same Figure. The λ parameter for Pb+Pb collisions is around 0.54, with no clear multiplicity dependence, similar to S+Nucleus collisions [8]. On the other hand, the source size parameters(R_{TS}, R_{TO} and R_L) are clearly increasing as a function of the charged multiplicity.

For the Pb+Pb system, R_L is larger than the transverse source size parameters, R_{TS} and R_{TO}, for all multiplicity intervals. The ratios of longitudinal to transverse source size parameters as a function of charged multiplicity are shown in Fig. 10. The ratios are almost constant as a function of the charged multiplicity. The averaged value of the ratio(R_L/R_{TS} and R_L/R_{TO}) in Pb+Pb system are 1.5±0.16 and 1.2±0.11, respectively. In the S+Nucleus system, these values are 1.2±0.12 and 1.1±0.10, respectively.

The duration of pion emission $\Delta\tau$ can be estimated from $\Delta\tau = \sqrt{(R_{TO}^2 - R_{TS}^2)}/\langle\beta_T\rangle$, where $\langle\beta_T\rangle$ is the mean transverse pion pair velocity. The value of the $\Delta\tau$ as a function of charged multiplicity is shown in Fig. 11. For the Pb+Pb data, this value is 3.8±1.2 fm/c and is consistent with the NA49 results [21]. The E866 experiment measuring 11.6 GeV/c per nucleon Au+Au collisions at BNL reported the duration of pion emission as 2-4 fm/c [22]. This implies negligible effect of incident energy on $\Delta\tau$. However, position-momentum correlations from expansion of the particle source could cause $\Delta\tau$ to underestimate the emission duration [23].

5 Discussion

NA44 has reported that the pion source size parameters in S+Nucleus collisions increase as a power function of charged multiplicity as

$$R_i = C \cdot (dN^{\pm}/d\eta)^{\alpha_i}, \tag{5}$$

and the extracted exponents(α_i) were about 0.2 [8]. The same kind of fits used for the S+Nucleus data were applied to combined S+Nucleus and Pb+Pb data. The solid curves in Fig. 9 are the results of fitting data points with (5). The fit parameters are shown in Table 5. The procedure results in rather poor fits. The power exponents extracted from these fits differ significantly from the 1/3 value expected in a scenario where freeze-out happens at constant density.

To check on the statistical significance and experimental coherence of the data, we have made additional analyses of the data.

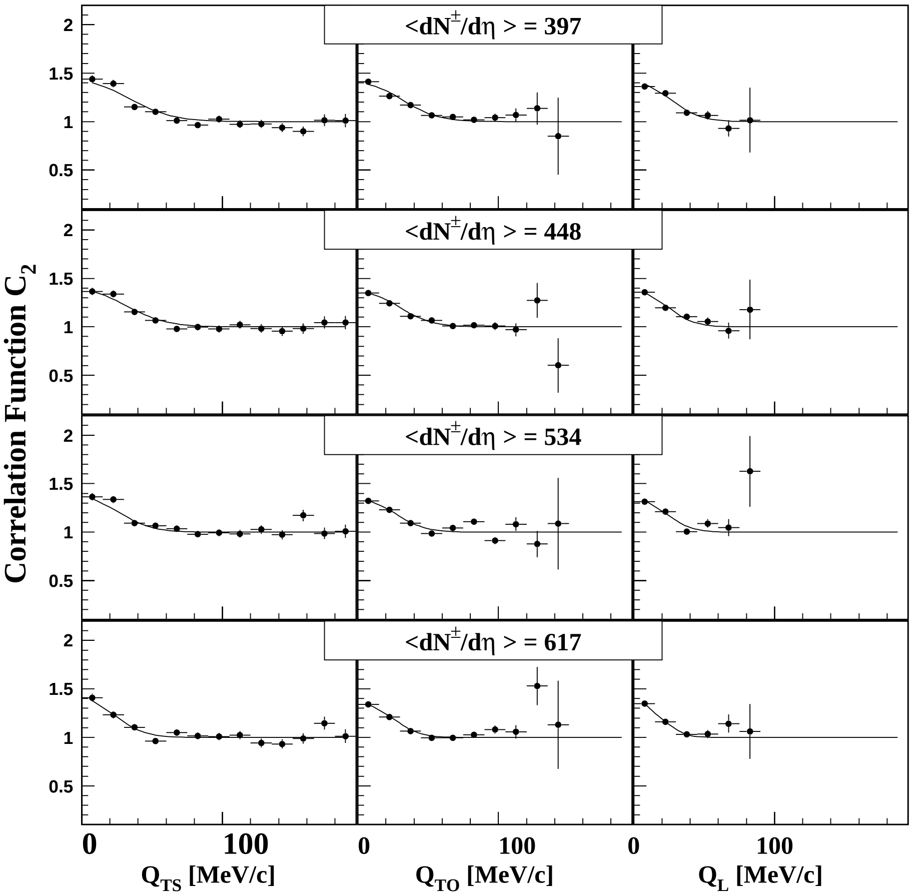

Fig. 7. Example of the projected correlation functions for the 44 mrad $\pi^-\pi^-$ data as a function of charged multiplicity. The projections are over the lowest 30 MeV/c in the other momentum difference directions

Table 4. Summary of the HBT source size parameters λ, R_{TS}, R_{TO} and R_L for pions as a function of the charged multiplicity. Uncertainties are statistical only. The S+S and S+Pb data were taken from [8]

System	$dN^{\pm}/d\eta$	λ	R_{TS} [fm]	R_{TO} [fm]	R_L [fm]	χ^2/DOF
S+S	20 ± 10	0.55 ± 0.02	2.95 ± 0.17	3.02 ± 0.13	4.01 ± 0.28	5668/5796
	44 ± 11	0.58 ± 0.02	3.87 ± 0.26	3.82 ± 0.16	3.59 ± 0.35	5124/5744
S+Pb	24 ± 10	0.57 ± 0.03	2.90 ± 0.19	3.39 ± 0.15	3.55 ± 0.30	5280/5925
	67 ± 13	0.56 ± 0.03	3.14 ± 0.19	3.90 ± 0.16	4.52 ± 0.33	5524/5976
	96 ± 9	0.60 ± 0.03	3.97 ± 0.26	3.94 ± 0.15	3.82 ± 0.31	5534/5972
	117 ± 12	0.61 ± 0.03	3.68 ± 0.32	4.69 ± 0.23	4.87 ± 0.35	4917/5842
Pb+Pb	304 ± 51	0.56 ± 0.03	4.07 ± 0.38	5.17 ± 0.31	6.29 ± 0.52	1763/1331
semi-central	455 ± 47	0.56 ± 0.04	4.50 ± 0.42	5.79 ± 0.39	6.74 ± 0.60	1498/1293
Pb+Pb	403 ± 25	0.52 ± 0.03	4.08 ± 0.27	4.71 ± 0.23	6.05 ± 0.41	1721/1649
Central	448 ± 17	0.51 ± 0.03	4.49 ± 0.28	5.15 ± 0.25	6.77 ± 0.49	2092/1733
	534 ± 17	0.53 ± 0.03	5.42 ± 0.40	5.95 ± 0.31	7.28 ± 0.48	2168/1718
	592 ± 28	0.66 ± 0.04	6.13 ± 0.48	6.80 ± 0.36	8.36 ± 0.57	1762/1545

Table 5. Parameters obtained from a fitting of the source size parameters with a power function of the charged multiplicity

	C	α_i	χ^2/DOF
R_{TS}	1.81 ± 0.38	0.15 ± 0.04	17/10
R_{TO}	1.84 ± 0.30	0.18 ± 0.03	22/10
R_L	1.65 ± 0.27	0.23 ± 0.03	18/10

– Beyond the fit shown in Table 5, we have fit the data for two separate multiplicity intervals. One is the low multiplicity region, which has $dN^{\pm}/d\eta$ less than 430 and includes the S+Nucleus results. The other is the high multiplicity region with $dN^{\pm}/d\eta$ greater than 430. The results for α_i obtained for the low multiplicity and the higher multiplicity region are shown in Table 6. The obtained α_i parameters for high mul-

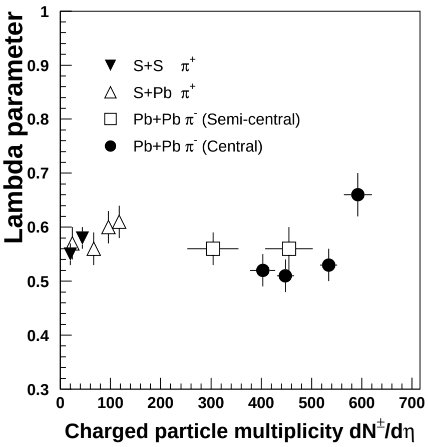

Fig. 8. Lambda parameter as a function of charged multiplicity for the $Pb{+}Pb \to \pi^-\pi^- + X$ and $S{+}Nucleus \to \pi^+\pi^+ + X$. Uncertainties are statistical only

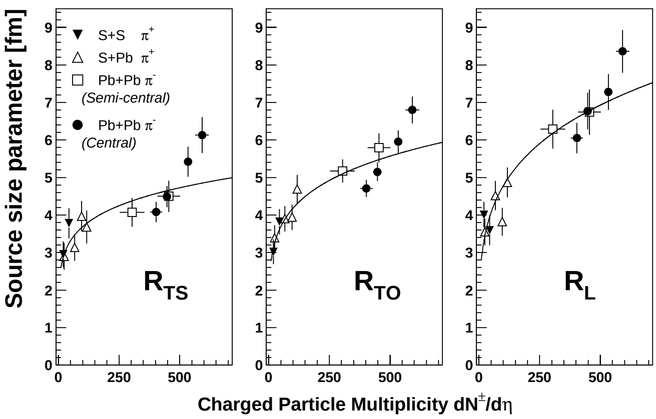

Fig. 9. The source size parameters as a function of charged multiplicity for the $Pb + Pb \to \pi^-\pi^- + X$ and $S + Nucleus \to \pi^+\pi^+ + X$. The solid line shows the results of fitting data points with a function $R = C \cdot (dN^{\pm}/d\eta)^{\alpha}$. Uncertainties are statistical only

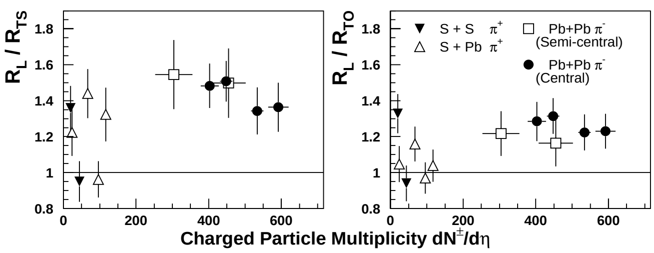

Fig. 10. The ratio of longitudinal to transverse source size parameters as a function of charged multiplicity. Uncertainties are statistical only

tiplicity regions are statistically different($> 4\sigma$) from the parameters obtained from fitting the low multiplicity data.

– We have combined the data from the three lowest multiplicity bins from central triggered data that have overlap with the upper half of the "semi-central" triggered data (see Fig. 6). The same three-dimensional

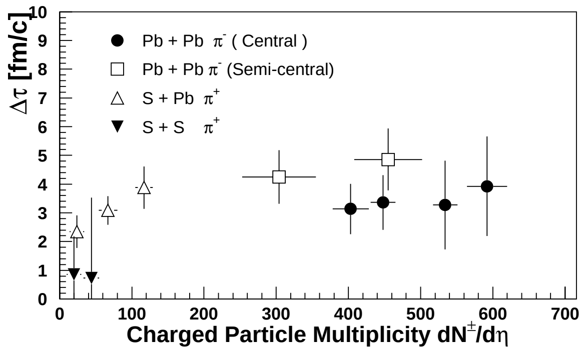

Fig. 11. The duration of pion emission $\Delta\tau$ as a function of charged multiplicity. Uncertainties are statistical only

analysis was applied to this data sample and the results are shown in Table 7. We observe that the results are agreement within errors with those obtained by the analysis of the higher part of the "semi-central" data removing the possibility of something being fundamentally wrong with the higher multiplicity data.

– We have also checked whether the sources of systematic errors could influence the obtained behavior. To that end, we have varied the two most important sources of systematic errors, i.e. systematic error by changing the Monte Carlo m_T slope parameters and changing number of hits on strip chambers(see Table 3). Varying these parameters does not change the observed trend because all the data points are affected in the same manner.

These tests indicate that no trivial explanation for the trend of the data is possible.

The measured increase of source size parameters with increasing charged multiplicity suggests that the freeze-out volume also increases. The radius parameters represent the source size of a homogeneous region; the true size of the system could be larger. We estimated the homogeneous volume as a cylinder with transverse radius R_{TS} and longitudinal dimension $2 \times R_L$. Figure 12 shows the estimated homogeneous volume as a function of charged multiplicity. The data points for the homogeneous volume are fitted by

$$V = C \cdot (dN^{\pm}/d\eta)^{\alpha_i}, \tag{6}$$

for "low multiplicity" and "high multiplicity" region, separately. The fit results are shown in Table 8. The low multiplicity shows good agreement with the curve extrapolated from S+Nucleus data, however, in the high multiplicity region, the trend as a function of charged multiplicity is significantly different from what we get by extrapolating S+Nucleus data. The assumption of freeze-out at constant density means that the homogeneous volume will linearly increase with charged multiplicity. However the data obviously do not follow such a trend.

Note that forcing the last lambda point in Fig.8 to level the other points will change the last Volume point down but within the error.

Table 6. Parameters obtained fitting the source size parameters with a power function of the charged multiplicity separately for both low and high multiplicity regions

	Low multiplicity region			High multiplicity region		
	C	α_i	χ^2/DOF	C	α_i	χ^2/DOF
R_{TS}	2.23 ± 0.40	0.10 ± 0.04	3.58/6	0.009 ± 0.004	1.02 ± 0.08	0.13/2
R_{TO}	2.20 ± 0.32	0.14 ± 0.03	5.60/6	0.04 ± 0.02	0.78 ± 0.06	2.05/2
R_L	2.01 ± 0.37	0.18 ± 0.04	9.87/6	0.10 ± 0.06	0.69 ± 0.09	0.54/2

Table 7. Source size parameters λ, R_{TS}, R_{TO} and R_L for pions using combined central triggered multiplicity bins. Uncertainties are statistical only

System	λ	R_{TS} [fm]	R_{TO} [fm]	R_L [fm]	χ^2/DOF
Combined data	0.52 ± 0.02	4.70 ± 0.18	5.28 ± 0.15	6.78 ± 0.27	2959/2183
higher half of semi-central data	0.56 ± 0.04	4.50 ± 0.42	5.79 ± 0.39	6.74 ± 0.60	1498/1293

Table 8. Parameters obtained fitting the source size volume ($2\pi R_{TS}^2 R_L$) with a power function of the charged multiplicity for both of low and high multiplicity regions

Low multiplicity region			High multiplicity region		
C	α	χ^2/DOF	C	α	χ^2/DOF
59.3 ± 18.6	0.40 ± 0.07	3.56/6	0.005 ± 0.005	1.97 ± 0.14	1.85/2

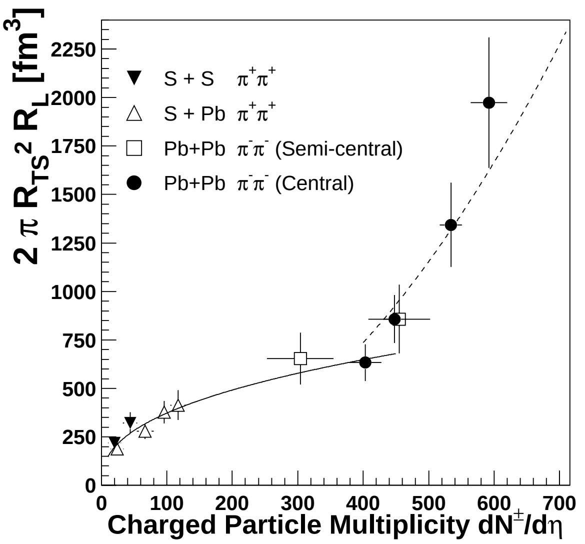

Fig. 12. The homogeneous volume of the source ($2\pi R_{TS}^2 \cdot R_L$) at freeze-out as a function of charged multiplicity. The solid(dotted) curve present fitted results for "low multiplicity(high multiplicity)" region with a function $V = C \cdot (dN^{\pm}/d\eta)^{\alpha}$. Uncertainties are statistical only

6 Conclusion

The systematic study of source size parameters as a function of charged multiplicity for negative pions created in Pb+Pb collisions has been done by means of two-particle interferometry. The sizes increase with increasing charged multiplicity.

The value of λ appears independent of charged multiplicity, $\lambda < 1$ could be explained the result of long-lived resonance decay(ω, η...etc.) [23]. Nearly identical λ parameters for both Pb+Pb data and S+Nucleus data imply that the fraction of pions from resonance decay does not change dramatically between S+Nucleus and Pb+Pb collisions.

For Pb+Pb collisions, R_L is larger than R_{TS} and R_{TO}, for all multiplicity intervals. These three parameters were approximately equal in S+Nucleus collisions. The ratios (R_L/R_{TS}) and (R_L/R_{TO}) are almost constant as a function of charged multiplicity and have values 1.5±0.16 and 1.2±0.11, respectively. The duration of pion emission $\Delta\tau$ is estimated for each multiplicity interval. The value of $\Delta\tau$ is almost constant as a function of the charged multiplicity in Pb+Pb collisions and has a value 3.8±1.1 fm/c.

It is interesting to note that within the limited statistics, the data points for Pb+Pb seems to indicate a stronger dependence on multiplicity than the S+Nucleus data. This occurs despite the fact that the increase in flow velocity from S+Nucleus to Pb+Pb [9] would tend to reduce the multiplicity dependence. In the present experiment neither the low nor high multiplicity data support the hypothesis of freeze-out at a constant density. In the multiplicity interval up to $dN^{\pm}/d\eta$=430, the analysis suggest a freeze-out at ever higher density, while for the high multiplicity intervals, the analysis suggests a dilution of the freeze-out density.

Acknowledgements. The NA44 collaboration wish to thank the staff of the CERN PS-SPS accelerator complex for their excellent work. We are also grateful for support given by the Danish Natural Science Research Council; the Japanese Society for the Promotion of Science; the Ministry of Education, Science and Culture, Japan; the Swedish Science Research Council; the Fond für Förderung der Wissenschaftlichen Forschung; the National Science Foundation; and the US Department of Energy.

References

1. T. Alber et al., NA49 Collab., Phys. Rev. Lett. **75** (1995) 3814
2. E. Laermann, Nucl. Phys. **A610** (1996) 1c
3. M.C.Abreu et al., NA50 Collab., Phys. Lett **B477** (2000) 28
4. E. Andersen et al., WA97 Collab., Phys. Lett **B449** (1999) 401
5. T. Matsui, H. Satz, Phys. Lett **B178** (1986) 416
6. P. Koch, B. Müller, and J. Rafelski, Phys. Rep. **B142** (1986) 167
7. S. Pratt, Phys. Rev. **D33** (1986) 1314
8. K. Kaimi et al., NA44 Collab., Z.Phys. **C75** (1997) 619
9. I.G. Bearden et al., NA44 Collab., Phys. Rev. Lett. **78** (1997) 2080
10. I.G. Bearden et al., NA44 Collab., Phys. Rev. **C58** (1998) 1656
11. A. Sakaguchi et al., NA44 Collab., Nucl. Phys. **A638** (1998) 103c
12. N. Maeda et al., Nucl. Instr. and Meth. **A346** (1994) 132
13. T. Kobayashi et al., Nucl. Instr. and Meth. **A287** (1990) 389
14. C.W. Fabjan et al., Nucl. Instr. and Meth. **A367** (1995) 240
15. S. Esumi et al., FIZIKA **B4** (1995) 205
16. A. Braem et al., Nucl. Instr. and Meth. **A409** (1998) 426
17. W.A. Zajc et al., Phys. Rev. **C29** (1984) 2173
18. K. Kadija, Phys. Lett. **B287** (1992) 362
19. H. Bøggild et al., NA44 Collab., Phys. Lett. **B302** (1993) 510
20. S. Pratt, Phys. Rev. **D33** (1986) 72
21. K. Kadija et al., NA49 Collab., Nucl. Phys. **A610** (1996) 248c
22. R.A. Saltz, M. Baker and J.H. Lee, Nucl. Phys. **A661** (1999) 439c
23. D.E. Fields et al., Phys. Rev. **C52** (1995) 866